eman ta zabal zazu

Universidad del País Vasco
Euskal Herriko Unibertsitatea

Modified Ehrenfest formalism: A new approach for large scale ab-initio molecular dynamics

Xavier Iago Andrade Valencia

Dpto. Física de Materiales
Universidad del País Vasco/Euskal Herriko Unibertsitatea

Memoria resumen
Prueba de suficiencia investigadora

26 de Noviembre 2008

Contents

Abstract 5

I. Introduction 7

II. Theory 10

A. Ehrenfest dynamics 10

B. Ehrenfest dynamics in TDDFT 14

C. Modified E-TDDFT formalism 15

1. Lagrangian and equations of motion 15

2. Symmetries and conserved quantities 17

3. Physical interpretation 19

4. Numerical properties 20

III. Methods 20

A. Real-space finite-difference method 20

B. Pseudopotential approximation 21

C. Calculation of the Forces 22

D. Time-propagation 22

E. Parallelization 23

IV. Results 24

A. Two band model 24

B. Nitrogen molecule 27

C. Benzene 27

D. Fullerene 30

V. Conclusions 30

Acknowledgements 33

References 34

Abstract

The application of first principles molecular dynamics to complex systems is hindered by the large number of atoms and the different time scales (femtoseconds to nanoseconds) to be spanned. This is particularly relevant for the description of many physical phenomena in nano-science, biology and material science. Therefore, the development of new algorithms and theories is required in order to achieve a description of these processes and systems from first principles. In this work, we present a new formalism that, due to its numerical properties, is ideal for simulating the molecular dynamics of systems containing thousands of atoms.

First principles molecular dynamics is usually performed in the framework of ground-state Born-Oppenheimer calculations or the Car-Parrinello scheme. The major drawback of both methods is the necessity to enforce the orthogonalization of the wave functions explicitly, making these methods computationally expensive for very large systems. Alternatively, one can handle the electron-ion dynamics within the Ehrenfest scheme where no explicit orthogonalization is necessary. However, in the Ehrenfest method the time steps need to be much smaller than in both the Born-Oppenheimer and the Car-Parrinello scheme. In the present work we preserve the desirable properties of the Ehrenfest scheme in a scheme that allows for a considerable increase of the time step while keeping the system close to the Born-Oppenheimer surface. We will show that the automatic orthogonalization is of fundamental importance for large systems because it reduces the scaling of the numerical cost with the number of particles and, in addition, allows for a very efficient parallelization, hence giving the method tremendous potential for applications in computational science.

The present work provides the formal details of the new method and its implementation in the real-space code Octopus. Comparisons with the widely used Car-Parrinello molecular dynamics method are made, both in terms of physical results and numerical cost, showing that the new approach is advantageous above a certain number of particles in the system. The method is not tied to a real-space implementation and can be transported to any representation, making it suitable for inclusion in any ab-initio molecular dynamics software.

The following peer-review articles are derived from this work:

- J. L. Alonso, X. Andrade, P. Echenique, F. Falceto, D. Prada and A. Rubio, Phys. Rev. Lett. **101** 096403 (2008).

- X. Andrade, A. Castro, D. Zueco, J. L. Alonso, P. Echenique, F. Falceto and A. Rubio, *to be submitted*, J. Chem. Theory Comput. (2009).

I. INTRODUCTION

In the last decades the concept of theoretical of atomistic simulations of complex structures in different fields of research (from material science in general, to biology) has emerged as a third discipline between theory and experiment. Computational science is now an essential adjunct to laboratory experiments, it provides high-resolution experiments that can guide research and serve as tools for discovery. Today computer simulations unified electronic structure and ion dynamics has come to an age although important challenges remain to be solved. This "Virtual lab" can provide valuable information about complex materials with refined resolution in space and time, allowing researchers to gain understanding about the microscopic and physical origins of materials behavior: from low-dimensianl nanostrcutures, to geology, atmospheric science, renewable energy, (nano)electronic devices, (supra)-molecular chemistry etc. Since the numerical approaches to handle those problems require "large-scale calculations" the success of this avenue of research was only possible in conjuntion with the development of high-performance computers[1]. The present work will address our recent developments in the field of first-principles Molecular Dynamics simulations, before getting into it we would like to frame the work from a historical perspective.

Molecular Dynamics (MD) consists of following the dynamics of a system of atoms or molecules governed by some interaction potential; in order to do so, "one could at any instant calculate the force on each particle by considering the influence of each of its neighbours. The trajectories could then be traced by allowing the particles to move under a constant force for a short-time interval and then by recalculating a new force to apply for the next short-time interval, and so on." This description was given by Alder and Wainwright in arguably the first report of such a computer-aided calculation[2] [3] in 1959 (probably the first so-called MD simulation for a model one-dimensional solid was done by Fermi et al in ref. [4] as discussed in [5]. We can still use this description to broadly define the scope of

[1] As stated by Dirac in 1929, "The fundamental laws necessary for the mathematical treatment of a large part of physics and the whole of chemistry are thus completely known, and the difficulties lies only in the fact that application of these laws leads to equations that are too complex to be solved"

[2] Computer simulations of the dynamics of systems of interacting molecules based on the Monte Carlo methods were presented some years before[1]. Also, before the work of Alder and Wainwright, some previous "computations" were reported that did not utilize modern computers, but rather real physical models of the system, i.e. rubber balls linked by rods[2]. The rapid improvement of digital computer machines discouraged this cumbersome, yet entertaining, methodology.

MD, although many variants and ground-breaking developments have appeared during these fifty years, addressing mainly two key issues: the limitation in the number of particles and time-scale that can be addressed, and the accuracy of the interaction potential, for further relevant works in the field of molecular simulations see for example Ref. [6].

The former issue was already properly stated by Alder and Wainwright: "The essential limitations of the method are due to the relatively small number of particles that can be handled. The size of the system of molecules is limited by the memory capacity of the computing machines." This statement is not obsolete, although the expression "small number of particles" has today of course a very different meaning – linked as it is to the exponentially growing capacities of computers.

The latter issue – the manner in which the atomic interaction potential is described – has also developed significantly over the years. Alder and Wainwright used solid impenetrable spheres in the place of atoms; nowadays, in the realm of the so-called "classical" MD one makes use of *force fields*: simple mathematical formulae are used to describe atomic interactions; the expressions are parameterised by fitting either to reference first-principles calculations or experimental data. These models have become extremely sophisticated and successful, although they are ultimately bound by a number of limitations. For example, it is difficult to tackle with electronic polarisation effects (charges were traditionally considered to be constant) and one needs to make use of polarisable models, whose transferability is very questionable but are widely used with success in many situations. Likewise, the force field models are constructed assuming a predetermined bond arrangement, disabling the option of chemical reactions – some techniques exist that attempt to overcome this restriction[7], but they are also difficult to transfer and must be carefully adapted to each particular system.

The road towards precise, non-empirical interatomic potentials reached its destination when the possibility of performing *ab initio* MD (AIMD) was realized[8, 9]. In this approach, the potential is not modelled a priori via some parametrized expression, but rather generated "on the fly" by performing accurate first-principles electronic structure calculations. The accuracy of the calculation is therefore limited by the level of theory used to obtain the electronic structure – although one must not forget that underlying all MD simulations is the electronic-nuclear separation *ansatz* ("adiabatic or Born-Oppenheimer approximation"), and the classical limit for the nuclei. The use of very accurate first principles methods for the electrons implies very large computational times, and therefore it is not surprising that

AIMD was not really born until density-functional theory (DFT) became mature – since it provides the necessary balance between accuracy and computational feasibility[10–13]. In fact, the term AIMD in most occasions refer exclusively to the technique proposed by Car and Parrinello in 1985[14], which is based on DFT, but which also introduces an ingenious acceleration scheme based on a fake electronic dynamics as a way to unify DFT and molecular dynamics. However, the term AIMD encompasses more possibilities – and in the present work will in fact discuss one of them.

As a matter of fact, the most obvious way to perform AIMD would be to compute the forces on the nuclei by performing electronic structure calculations on the ground-state Born-Oppenheimer potential energy surface. This we can call ground-state Born Oppenheimer MD (gsBOMD). It implies a demanding electronic minimisation at each step and schemes using time-reversible integrators have been recently developed[15]. The Car-Parrinello (CP) technique is in fact a scheme that allows to propagate the Kohn-Sham (KS) orbitals with a fictitious dynamics that nevertheless mimics gsBOMD – bypassing the need for the expensive minimisation. This idea has produced an enormous impact, allowing for succesful applications in a surprisingly wide range of areas[16]. Still, it implies a substantial cost, and many interesting potential applications have been frustrated due to the impossibility of attaining the necessary system size or simulation time length. There have been several efforts to refine or redefine the CP scheme in order to enhance its power: linear scaling methods[17] attempt to speed-up in general any electronic structure calculation; the use of a localised orbital representation (instead of the much more common plane-waves utilised by CP practitioners) has also been proposed; recently, Kühne and coworkers[18] have proposed an approach which is based on CP, but which allows for sizable gains in efficiency. In any case, the cost associated with the orbital orthonormalisation that is required in any CP-like procedure is a potential bottleneck that hinders its application to very large-scale simulations.

Another possible AIMD strategy is Ehrenfest MD, to be presented in the following section. In this case, the electron-nuclei separation *ansatz* and the Wentzel-Kramers-Brillouin[19–21] (WKB) classical limit are also considered; however, the electronic subsystem is not assumed to evolve adiabatically on one of the potential energy surfaces (PES) – typically the ground-state one. This permits the electrons to move between PES, and to evolve on linear combinations of adiabatic states. As a drawback, the time-step required for a

simulation in this scheme is determined by the electronic frequencies, which means about three orders of magnitude less than the time scale required to follow the nuclei in a BOMD.

If one wants to do Ehrenfest-MD, the traditional "ground-state" DFT is not enough, and one must rely on time-dependent density-functional theory[22, 23]. Coupling TDDFT to the EMD idea provides with an orthogonalisation-free alternative to CP AIMD – plus it allows for excited-states AIMD. If the system is such that the gap between the ground-state and the excited states is large, Ehrenfest-MD tends to gsAIMD. The advantage provided by the lack of need of orthonormalisation is unfortunately offset by the smallness of the required time-step. Recently, some of the authors of the present article have presented a formalism for large scale AIMD based on EMD and TDDFT, that borrows some of the ideas of CP in order to increase this time step and make TDDFT-EMD competitive with CP[24].

This article intends to be a more detailed description of this proposed methodology: we will start, in Section II A by revisiting the mathematical route that leads from the full many-particle electronic and nuclear Schrödinger equation to the EMD model, as well as its possible marriage with TDDFT. Section II C presents in detail the aforementioned novel formalism, along with a discussion regarding symmetries and conservation laws. Sections III and **??** are dedicate to the numerical technicalities, including several application examples.

II. THEORY

A. Ehrenfest dynamics

The starting point is the time-dependent Schrödinger equation (atomic units [25] are used throughout this paper) for a molecular system described by the wavefunction $\Phi\big(\{x_j\}_{j=1}^n, \{X_J\}_{J=1}^N, t\big)$:

$$i\dot{\Phi}\big(\{x_j\}_{j=1}^n, \{X_J\}_{J=1}^N, t\big) = \hat{H}\Phi\big(\{x_j\}_{j=1}^n, \{X_J\}_{J=1}^N, t\big) \ , \tag{1}$$

where the dot indicates the time derivative, and we denote as $\mathbf{r}_j$, σ_j, and $\mathbf{R}_J$, Σ_J the Euclidean coordinates and the spin of the j-th electron and the J-th nuclei, respectively, with $j = 1, \ldots, n$, and $J = 1, \ldots, N$. We also define $x_j = (\mathbf{r}_j, \sigma_j)$, and $X_J = (\mathbf{R}_J, \Sigma_J)$, and we shall denote the whole sets $r = \{\mathbf{r}_j\}_{j=1}^n$, $R = \{\mathbf{R}_J\}_{J=1}^N$, $x = \{x_j\}_{j=1}^n$, and $X = \{X_J\}_{J=1}^N$, using single letters in order to simplify the expressions.

The molecular Hamiltonian operator is defined as

$$\begin{aligned}\hat{H} &= -\sum_J \frac{1}{2M_J}\nabla_J^2 - \sum_j \frac{1}{2}\nabla_j^2 + \sum_{J<K} \frac{Z_J Z_K}{|\mathbf{R}_J - \mathbf{R}_K|} + \sum_{j<k} \frac{1}{|\mathbf{r}_j - \mathbf{r}_k|} - \sum_{J,j} \frac{Z_J}{|\mathbf{R}_J - \mathbf{r}_j|} \\ &= -\sum_J \frac{1}{2M_J}\nabla_J^2 - \sum_j \frac{1}{2}\nabla_j^2 + \hat{V}_{\mathrm{n-e}}(r,R) \\ &= -\sum_J \frac{1}{2M_J}\nabla_J^2 + \hat{H}_{\mathrm{e}}(r,R) \ , \end{aligned} \tag{2}$$

where all sums must be understood as running over the whole natural set for each index, unless otherwise specified. M_J is the mass of the J-th nucleus in units of the electron mass, and Z_J is the charge of the J-th nucleus in units of (minus) the electron charge. Also note that we have defined the nuclei-electrons potential $\hat{V}_{\mathrm{n-e}}(r,R)$ and the electronic Hamiltonian $\hat{H}_{\mathrm{e}}(r,R)$ operators.

The initial conditions of eq. (1) are given by

$$\Phi^0 = \Phi(x,X,0) \ , \tag{3}$$

and we assume that $\Phi(x,X,t)$ vanishes at infinity $\forall t$.

Now, to derive the quantum-classical molecular dynamics (QCMD) known as Ehrenfest molecular dynamics (EMD) from the above setup, one starts with a separation ansatz for the wavefunction $\Phi(x,X,t)$ between the electrons and the nuclei [26, 27], leading to the so-called time-dependent self-consistent-field (TDSCF) equations [8, 28, 29]. The next (and last) step is to approximate the nuclei as classical point particles via short wave asymptotics, or WKB approximation [8, 28, 29]. The resultant EMD scheme is contained in the following system of coupled differential equations [28, 29]:

$$i\dot{\psi}(x,t) = \hat{H}_{\mathrm{e}}(r,R)\psi(x,t) \tag{4}$$

$$M_J\ddot{\mathbf{R}}_J(t) = -\int \mathrm{d}x\psi^*(x,t)\left[\nabla_J \hat{H}_{\mathrm{e}}\big(r;R(t)\big)\right]\psi(x,t) \ , \tag{5}$$

where $\psi(x,t)$ is the wavefunction of the electrons, $\mathbf{R}_J(t)$ are the nuclear trajectories, and we have used $\mathrm{d}x$ to indicate integration over all spatial electronic coordinates and summation over all electronic spin degrees of freedom. Also, a semicolon has been used to separate the r from the $R(t)$ in the electronic Hamiltonian, in order to stress that only the latter are actual time-dependent degrees of freedom the system.

The initial conditions in EMD are given by

$$\psi^0 \;=\; \psi(x,0) \tag{6}$$

$$\mathbf{R}_J^0 \;=\; \mathbf{R}_J(0)\;, \quad \dot{\mathbf{R}}_J^0 = \mathbf{R}_J(0)\;, \tag{7}$$

and we assume that $\psi(x,t)$ vanishes at infinity $\forall t$.

Also note that, since in this scheme $\{\mathbf{R}_J, \psi\}$ is a set of independent variables, we can rewrite eqs. (III C) as

$$M_J \ddot{\mathbf{R}}_J(t) = -\nabla_J \int \mathrm{d}x \psi^*(x,t) \hat{H}_\mathrm{e}\big(r; R(t)\big) \psi(x,t)\;, \tag{8}$$

a fact which is similar in form, but unrelated to the Hellmann-Feynman theorem[3]. As pointed out by Tully [34], it is likely that the confusion about whether eqs. (8) should be used to define the EMD, or the gradient must be applied to the electronic Hamiltonian inside the integral, as in (III C), has arisen from applications in which $\psi(x,t)$ is expressed as a finite expansion in the set of adiabatic basis functions, $\eta_a(x;R)$, defined as the eigenfunctions[4] of $\hat{H}_\mathrm{e}(r;R)$:

$$\hat{H}_\mathrm{e}(r;R)\eta_a(x;R) = E_a(R)\eta_a(x;R)\;. \tag{9}$$

The use of a precise notation, such as the one introduced in this section, helps to avoid this kind of confusions. An example of a misleading notation in this context would consist in writing $\psi(r,R,t)$ for the electronic wavefunction [34, 35], when, as we have emphasized, there exists no explicit dependence of ψ on the nuclear positions R.

Although the approach underlying EMD is clearly a mean-field theory, transitions between electronic adiabatic states are included in the scheme, this can be made evident by performing the following change of coordinates from $\{\psi, R\}$ to $\{c, R'\}$ (with $c = \{c_a\}_{a=1}^{\infty}$):

$$\psi(x,t) \;=\; \sum_a c_a(t)\eta_a\big(x; R'(t)\big) \tag{10}$$

$$\mathbf{R}_J(t) \;=\; \mathbf{R}'_J(t)\;, \tag{11}$$

where $\eta_a(x;R)$ are known functions given by (9) and, even if the transformation between the R and the R' is trivial, we have used the prime to emphasize that there are two distinct

[3] Perhaps the first detailed derivation of the so-called Hellmann-Feynman theorem was given by Güttinger [30], The theorem had nevertheless been used before that date[31]. The derivations of Hellmann[32] and Feynman[33], who named the theorem, came a few years afterwards.

[4] In general, $\{\eta_a(x;R)\}$ may contain a discrete and a continuous part. However, in this manuscript, we will forget the continuous part in order to simplify the mathematics.

sets of independent variables: $\{\psi, R\}$ and $\{c, R'\}$. This is very important if one needs to take partial derivatives, since a partial derivative with respect to a given variable is only well defined when the independent set to which that variable belongs is specified[5]. For example, a possible mistake is to assume that, since c_a 'is independent of' $\mathbf{R}'_J$, and $\mathbf{R}_J = \mathbf{R}'_J$, then c_a 'is also independent' of $\mathbf{R}_J$ and, therefore, the unprimed partial derivative $\nabla_J c_a$ is zero. The flaw in this reasoning is that the unprimed partial derivative ∇_J is defined to be performed at constant ψ, and not at constant c, since the relevant set of independent variables is $\{\psi, R\}$. In fact, if we write the inverse transformation

$$c_a(t) \;=\; \int \mathrm{d}x \psi^*(x,t) \eta_a\big(x; R(t)\big) \;, \tag{12}$$

$$\mathbf{R}'_J(t) \;=\; \mathbf{R}_J(t) \;, \tag{13}$$

we can clearly appreciate that, even if it is independent from R' by construction, c_a is neither independent from ψ, nor from R.

On the other hand, if we truncated the sum in (10), then there would appear an explicit dependence of ψ on R and the state of affairs would be different, since $\{\psi, R\}$ would no longer be a set of independent variables. However, in the context of an exact (infinite) expansion in (10), the right hand sides of eqs. (III C) and (8) are equal, as we mentioned before, and we do not have to worry about which one is more appropriate. It is in this infinite-adiabatic basis situation that we will now use eq. (III C) and the expansion in (10) to illustrate the non-adiabatic character of EMD.

If we perform the change of variables described in eqs. (10) to the EMD eqs. (4), and we use that

$$\nabla_J \hat{H}_{\mathrm{e}}(r; R) = \nabla'_J \hat{H}_{\mathrm{e}}(r; R') \;, \tag{14}$$

we see that we will have to calculate terms of the form

$$\int \mathrm{d}x \eta^*_a\big(x; R'(t)\big) \nabla'_J \hat{H}_{\mathrm{e}}\big(r; R'(t)\big) \eta_b\big(x; R'(t)\big) \;, \tag{15}$$

which can be easily extracted from the relation

$$\nabla'_J \int \mathrm{d}x \eta^*_a\big(x; R'(t)\big) \hat{H}_{\mathrm{e}}\big(r; R'(t)\big) \eta_b\big(x; R'(t)\big) = \nabla'_J E_a\big(R'(t)\big) \delta_{ab} \;. \tag{16}$$

[5] In the development of the classical formalism of Thermodynamics, this point is crucial.

In this way, we obtain for the nuclear EMD equation

$$M_J\ddot{\mathbf{R}}'_J(t) \;=\; -\sum_a |c_a(t)|^2\nabla'_J E_a\big(R'(t)\big) \\ -\sum_{a,b} c_a^*(t)c_b(t)\left[E_a\big(R'(t)\big) - E_b\big(R'(t)\big)\right]\mathbf{d}_J^{ab}\big(R'(t)\big)\;, \tag{17}$$

where the non-adiabatic couplings (NACs) are defined as

$$\mathbf{d}_J^{ab}\big(R'(t)\big) = \int \mathrm{d}x\eta_a^*\big(x;R'(t)\big)\nabla'_J\eta_b\big(x;R'(t)\big)\;. \tag{18}$$

To obtain the new electronic EMD equation, we perform the change of variables to (4) and we then multiply by $\eta_b^*\big(x;R'(t)\big)$ the resulting expression and integrate over the electronic coordinates x. Proceeding in this way, we arrive to

$$i\hbar\dot{c}_a(t) = E_a\big(R'(t)\big)c_a(t) - i\hbar\sum_b c_b(t)\left[\sum_J \dot{\mathbf{R}}'_J(t)\cdot\mathbf{d}_J^{ab}\big(R'(t)\big)\right]\;. \tag{19}$$

In the nuclear eqs. (17), we can see that the term depending on the moduli $|c_a(t)|^2$ directly couple the population of the adiabatic states to the nuclei trajectories, whereas interferences between these states are included via the $c_a^*(t)c_{b\neq a}(t)$ contributions. Analogously, in the electronic equations above, the first term represents the typical evolution of the coefficient of an eigenstate of the Hamiltonian, but, differently from the full quantum case, in EMD, the second term couples the evolution of all states with each other's through the velocity of the classical nuclei and the NACs.

B. Ehrenfest dynamics in TDDFT

Also in the framework of time-dependent density-functional theory (TDDFT), one can implement EMD. In fact, starting by an extension [36] of the Runge-Gross theorem [37] to arbitrary multicomponent systems, one can develop a TDDFT [38] for the system of electrons and nuclei described by (1). Then, after a classical treatment of nuclear motion and an approximation analogous to the self-interaction correction (SIC) scheme of Perdew and Zunger [39], one arrives to an Ehrenfest-TDDFT (E-TDDFT) dynamics, also obtainable from the following Lagrangian [24, 38, 40]:

$$L\big[\varphi(t),\dot{\varphi}(t),R(t),\dot{R}(t)\big] \;=\; \frac{i}{2}\sum_A\int \mathrm{d}\mathbf{r}\big(\varphi_A^*(\mathbf{r},t)\dot{\varphi}_A(\mathbf{r},t) - \dot{\varphi}_A^*(\mathbf{r},t)\varphi_A(\mathbf{r},t)\big) \\ +\sum_J\frac{M_J}{2}\dot{\mathbf{R}}_J(t)\cdot\dot{\mathbf{R}}_J(t) - E_{\mathrm{KS}}\big[\varphi(t),R(t)\big]\;, \tag{20}$$

where we have denoted by $\varphi = \{\varphi_A\}_{A=1}^{n/2}$, the whole set of Kohn-Sham (KS) orbitals of a closed-shell molecule, and $E_{\rm KS}[\varphi, R]$ is the KS energy:

$$E_{\rm KS}[\varphi, R] = 2\sum_A \int {\rm d}\mathbf{r}\varphi_A^*(\mathbf{r},t)\left(-\frac{\nabla^2}{2}\right)\varphi_A(\mathbf{r},t) - \int {\rm d}\mathbf{r}\sum_J\left(\frac{Z_J}{|\mathbf{R}_J(t)-\mathbf{r}|}\right)\rho(\mathbf{r},t) + \frac{1}{2}\int {\rm d}\mathbf{r}{\rm d}\mathbf{r}'\frac{\rho(\mathbf{r},t)\rho(\mathbf{r}',t)}{|\mathbf{r}-\mathbf{r}'|} + E_{\rm XC}\big[\rho(\mathbf{r},t)\big] + \sum_{J<K}\frac{Z_J Z_K}{|\mathbf{R}_J(t)-\mathbf{R}_K(t)|}\ , \quad (21)$$

where $E_{\rm XC}\big[\rho(\mathbf{r})\big]$ is the exchange-correlation energy, and the time-dependent electronic density is defined as

$$\rho(\mathbf{r},t) = 2\sum_A \big|\varphi_A(\mathbf{r},t)\big|^2\ . \quad (22)$$

In the following section, we introduce a modification of the E-TDDFT dynamics obtained from (20) aimed to the study of situations in which the contribution of the electronic excited states to the nuclei dynamics is negligible, i.e., situations in which one is interested in performing ground-state Born-Oppenheimer molecular dynamics (gsBOMD) [8].

C. Modified E-TDDFT formalism

1. *Lagrangian and equations of motion*

The whole new scheme can be obtained from the following Lagrangian

$$L[\varphi,\dot\varphi,R,\dot R] = \mu\frac{i}{2}\sum_A\int {\rm d}\mathbf{r}(\varphi_A^*(\mathbf{r},t)\dot\varphi_A(\mathbf{r},t) - \dot\varphi_A^*(\mathbf{r},t)\varphi_A(\mathbf{r},t)) + \sum_J\frac{M_J}{2}\dot{\mathbf{R}}_J\cdot\dot{\mathbf{R}}_J - E_{\rm KS}[\varphi,R]\ , \quad (23)$$

where we have ommited the spatial and time dependence of the objects for the sake of notational brevity.

Note that the major modification with respect to the E-TDDFT Lagrangian in (20) is the presence of a parameter μ that rescales of the electronic velocities. Since we are using atomic units, this is equivalent to changing $\hbar$ by a factor μ, but only in the electronic E-TDDFT equations (E-TDDFT is recovered when $\mu = 1$), which are obtained, together with the nuclear ones, as the equations of motion (EoM) of the new Lagrangian in (23):

$$i\,\mu\dot\varphi_A(\mathbf{r},t) = \frac{\delta E_{\rm KS}[\varphi,R]}{\delta\varphi_A^*(\mathbf{r},t)} = -\frac{1}{2}\nabla^2\varphi_A(\mathbf{r},t) + v_{\rm eff}[\varphi,R]\varphi_A \quad (24)$$

$$M_J\ddot{\mathbf{R}}_J = -\nabla_J E_{\rm KS}[\varphi,R]\ , \quad (25)$$

where v_{eff} is the time-dependent KS effective potential.

Compare with the gsBOMD Lagrangian:

$$L_{\text{BO}}[\varphi, R, \dot{R}] = \sum_J \frac{M_J}{2}\dot{\mathbf{R}}_J \cdot \dot{\mathbf{R}}_J - E_{\text{KS}}[\varphi, R] + \sum_{AB} \Lambda^{\text{BO}}_{AB} \left(\int \mathrm{d}\mathbf{r} \varphi^*_A(\mathbf{r}, t)\varphi_B(\mathbf{r}, t) - \delta_{AB} \right) , \quad (26)$$

and the corresponding EoM:

$$-\frac{1}{2}\nabla^2\varphi_A(\mathbf{r}, t) + v_{\text{eff}}[\varphi, R]\varphi_A(\mathbf{r}, t) = \sum_B \Lambda^{\text{BO}}_{AB}\varphi_B(\mathbf{r}, t) \quad (27)$$

$$\int \mathrm{d}\mathbf{r}\, \varphi^*_A(\mathbf{r}, t)\varphi_B(\mathbf{r}, t) = \delta_{AB} \quad (28)$$

$$M_J\ddot{\mathbf{R}}_J = -\nabla_J E_{\text{KS}}[\varphi, R] , \quad (29)$$

where $\Lambda^{\text{BO}} = (\Lambda^{\text{BO}}_{AB})$ is an Hermitian matrix of time-dependent Lagrange multipliers that ensure that the orbitals φ form an orthonormal set at each instant of time. The Euler-Lagrange equations corresponding to Λ^{BO}_{AB} in (28) are exactly these orhonormality constraints, and, together with eq. (27), constitute the time-independent KS equations. Therefore, assuming no metastability issues in the optimization problem, we have that the orbitals φ are completely determined[6] by the nuclear coordinates R, being in fact the BO ground state (gs), $\varphi = \varphi^{\text{gs}}(R)$, which allows us to write the EoM for gsBOMD in a much more compact and familiar form:

$$M_J\ddot{\mathbf{R}}_J = -\nabla_J E_{\text{KS}}\left[\varphi^{\text{gs}}(R), R\right] . \quad (30)$$

We can also compare the new dynamics with CPMD, whose Lagrangian reads

$$\begin{aligned} L_{\text{CP}}[\varphi, \dot{\varphi}, R, \dot{R}] = {} & \frac{1}{2}\mu_{\text{CP}} \sum_A \int \mathrm{d}\mathbf{r} |\dot{\varphi}_A(\mathbf{r}, t)|^2 + \sum_J \frac{M_J}{2}\dot{\mathbf{R}}_J \cdot \dot{\mathbf{R}}_J \\ & - E_{\text{KS}}[\varphi, R] + \sum_{AB} \Lambda^{\text{CP}}_{AB} \left(\int \mathrm{d}\mathbf{r} \varphi^*_A(\mathbf{r}, t)\varphi_B(\mathbf{r}, t) - \delta_{AB} \right) , \end{aligned} \quad (31)$$

and the corresponding EoM are

$$\mu_{\text{CP}}\ddot{\varphi}_A(\mathbf{r}, t) = -\frac{1}{2}\nabla^2\varphi_A(\mathbf{r}, t) + v_{\text{eff}}[\varphi, R] + \sum_B \Lambda^{\text{CP}}_{AB}\varphi_B(\mathbf{r}, t) \quad (32)$$

$$\int \mathrm{d}\mathbf{r} \varphi^*_A\varphi_B(\mathbf{r}, t) = \delta_{AB} \quad (33)$$

$$M_J\ddot{\mathbf{R}}_J = -\nabla_J E_{\text{KS}}[\varphi, R] , \quad (34)$$

[6] This fact is not in contradiction with the above discussion about coordinates independence. The difference between EMD and gsBOMD is that in the Lagrangian for the latter, the orbitals 'velocities' $\dot{\varphi}$ do not appear, thus generating eqs. (27) and (28), which can be regarded as *constraints* between the ψ and the R.

where $\Lambda^{\rm CP} = (\Lambda^{\rm CP}_{AB})$ is again an Hermitian matrix of time-dependent Lagrange multipliers that ensure the orthonormality of the orbitals φ, and $\mu_{\rm CP}$ is a fictitious electrons 'mass' which plays a similar role to the parameter μ in our new dynamics.

2. Symmetries and conserved quantities

In the following we shall study the conserved quantities associated to the global symmetries of the Lagrangian in (23) and we shall compare them with those of gsBOMD and CPMD. We shall be also interested in a gauge symmetry that is the key to understand the behaviour of (23) in the limit $\mu \to 0$ and its relation with gsBOMD.

The first symmetry we want to discuss is the time translation invariance of (23). This is easily recognized as L does not depend explicitly on time. Associated to this invariance there is an 'energy' conserved. Namely, using Noether theorem we have that

$$E = \sum_A \int \mathrm{d}\mathbf{r} \left(\frac{\delta L}{\delta \dot\varphi_A} \dot\varphi_A + \frac{\delta L}{\delta \dot\varphi^*_A} \dot\varphi^*_A \right) + \sum_{J,p} \frac{\partial L}{\partial \dot R^p_J} \dot R^p_J - L = \sum_J \frac{1}{2} M_J \dot R^2_J + E_{KS}[\varphi, R] \qquad (35)$$

is constant under the dynamics given by (III D), where $p = 1, 2, 3$ indexes the Euclidean coordinates of vectors $\dot{\mathbf{R}}_J$ (and $\mathbf{R}_J$ if needed).

Notice that E does not depend on the unphysical parameter μ and actually coincides with the exact energy that is conserved in gsBOMD. The situation is different in CPMD. There, we also have time translation invariance but the constant of motion reads

$$E_{CP} = \int \mathrm{d}\mathbf{r} \sum_A \frac{1}{2} \mu_{\rm CP} \dot\varphi^*_A(\mathbf{r}, t) \dot\varphi_A(\mathbf{r}, t) + E \ , \qquad (36)$$

which has the drawback that it depends on the unphysical 'mass' of the electrons, $\mu_{\rm CP}$, and its conservation implies that the physical energy E varies in time.

The second global symmetry we want to consider is the change of orthonormal basis of the space spanned by $\{\varphi_A\}_{A=1}^{n/2}$. Namely, given a Hermitian matrix S_{AB} ($S^+ = S$), we define the following transformation:

$$\varphi'_A = \sum_B \left(\mathrm{e}^{iS} \right)_{AB} \varphi_B \ . \qquad (37)$$

The Lagrangian in (23) depends on φ only through $\rho = 2 \sum_A |\varphi_A|^2$ and $\sum_A \varphi^*_A \dot\varphi_A$. Provided the matrix S is Hermitian and constant in time, both expressions are left unchanged by the transformation. Hence, we can invoke again Noether theorem to obtain a new conserved

quantity that reads

$$i\sum_{A,B}\int\left(\frac{\delta L}{\delta\dot{\varphi}_A}S_{AB}\varphi_B-\frac{\delta L}{\delta\dot{\varphi}_A^*}S_{AB}\varphi_B^*\right)=i\mu\sum_{A,B}\int\varphi_A^*S_{AB}\varphi_B\ . \tag{38}$$

Observe that we have a constant of motion for any Hermitian matrix S. This permits us to combine different choices in order to obtain that

$$\mu\int \mathrm{d}\mathbf{r}\varphi_A^*(\mathbf{r},t)\varphi_B(\mathbf{r},t)=\text{constant}\ . \tag{39}$$

In other words, if we start with an orthonormal set of wave functions φ and we let evolve the system according to (III D), the family of wave functions maintain its orthonormal character along time.

We would like to mention here that the above property is sometimes attributed on a supposed unitarity of the evolution [8, 40, 41]. Simply noticing that the evolution of φ is not linear as both (24) and (25) are non-linear equations, and that unitary evolution requires linearity, one can discard this argument.

We consider now the fate of (39) when $\mu\to 0$. We see that the constant of motion vanishes in that limit and, in fact, one can easily see that the orthonormality of φ is not preserved by eqs (III D) when μ is set to zero.

As we have seen in the previous section, both in gsBOMD and CPMD φ is defined to be an orthonormal set and, in order to fulfill this condition, one adds the corresponding Lagrange multipliers to the EoM. When performing numerical simulations, it is necessary to go through a computationally costly process of orthonormalization of φ at every step. In the dynamics that we propose, this orthonormalization is not required, making the numerical implementation more efficient.

There is however a delicate point here that is worth discussing. The issue is that the $\mu\to 0$ limit of our dynamics should correspond to gsBOMD in eqs. (27) (which includes Lagrange multipliers the and orthonormalization process), but the Lagrangian in (23) does not contain any multipliers and in fact they are unnecessary, as our evolution preserves the orthonormalization. This may rise some doubts on the equivalence between gsBOMD and the limit of vanishing μ of our dynamics.

To settle the issue we introduce the dynamical fields $\Lambda=(\Lambda_{AB})$, corresponding to Lagrange multipliers, in our Lagrangian, i.e.,

$$\tilde{L}[\varphi,\dot{\varphi},R,\dot{R},\Lambda]=L[\varphi,\dot{\varphi},R,\dot{R}]+\sum_{AB}\Lambda_{AB}\left(\int \mathrm{d}\mathbf{r}\varphi_A^*(\mathbf{r},t)\varphi_B(\mathbf{r},t)-\delta_{AB}\right)\ . \tag{40}$$

This modification has an important consequence: the global symmetry in (37) becomes a gauge one with the parameter of the tranformation depending on time. Actually one can easily verify that $\tilde{L}$ is invariant under

$$\varphi' = \mathrm{e}^{iS}\varphi \ , \tag{41}$$

$$\Lambda' = \mathrm{e}^{iS}\Lambda\mathrm{e}^{-iS} - \mu\mathrm{e}^{iS}\frac{\mathrm{d}}{\mathrm{d}t}\mathrm{e}^{-iS} \ . \tag{42}$$

This implies that, for $\mu \neq 0$, the fields Λ_{AB} can be transformed to any desired value by suitably choosing the gauge parameters $S_{AB}(t)$. Their value is therefore irrelevant and one could equally well take $\Lambda = 0$ or $\Lambda = \Lambda^{\mathrm{BO}}$ (the value it has in gsBOMD) without affecting any physical observable. This solves the puzzle and shows that the $\mu \to 0$ limit of the dynamics of (III D) is in fact gsBOMD.

3. Physical interpretation

By writing the left hand side of (24) as

$$\mu\frac{d\phi}{dt} = \frac{d\phi}{dt_e} \ , \tag{43}$$

equation (24) can be seen as a standard Ehrenfest equation in terms of a fictitious time.

From here is easy to see that the effect of μ is to scale the TDDFT ($\mu = 1$) excitation energies by a $1/\mu$ factor. So for $\mu > 1$ the gap of the artificial system is decreased, increasing the non-adiabatic coupling, while for small values of μ, the excited states are pushed up in energy forcing the system to stay in the adiabatic regime. This gives a physical explanation to the $\mu \to 0$ limit shown before.

If we now the propagation cost and the maximum time step for standard Ehrenfest dynamics, we can estimate that the maximum time step as a function of μ is

$$\Delta t\,(\mu) = \mu\,\Delta t\,(\mu = 1) \ . \tag{44}$$

By taking into account these two results we can see that there is a trade-off in the value of mu: low values will give physical accuracy while large values will produce a faster propagation.

The optimum value, that we will call μ_{max}, is the maximum value of μ that still keeps the system near the adiabatic regime. It reasonable to expect that this value is given by

the ratio between the electronic gap and the highest vibration energy in the system. For many systems, like some molecules or insulators, this ratio is large and we can expect large improvements with respect to standard EMD. For other systems, like metals, this ratio is small or zero and our method will not work well without modifications (that are presently being worked on). We note that a similar problem appears in the application of CP to these systems.

4. Numerical properties

From the numerical point of view our method inherits the main advantage of Ehrenfest dynamics, since propagation preserves orthogonality of the wave-function, it needs not be imposed and the numerical cost is proportional to $N_W N_C$ (with N_W the number of orbitals and N_C the number of grid points or basis set coefficients). For CP a re-orthogonalization has to be done, so the cost is proportional to $N_W^2 N_C$. From these scaling properties we can predict that for large enough systems our method will be less costly than CP. As we will show in section IV this crossover can occur for less than 1000 atoms.

Due to the complex nature of the propagator, Ehrenfest dynamics has to be performed using complex wave-functions. In CP real wave-functions can be used if the system is finite (without a magnetic field) or if the system is a supercell using only the gamma point. With respect to CP the actual number of degrees of freedom to be treated is the same, since CP equations are second order a second field has to be stored, either the artificial "velocity" of the wave-functions or the wave-function of the previous step.

III. METHODS

A. Real-space finite-difference method

The scheme described was implemented in the Octopus code[42, 43]. Octopus uses a real-space grid based representation combined with finite differences approximation for the calculation of derivatives[44, 45]. This representation has several advantages over other more traditional basis set schemes as plane waves, gaussian or atomic orbitals:

- The most adequate boundary conditions can be chosen. Usually this implies zero-

boundary conditions for finite systems and periodic boundary conditions for crystals and liquids, but also more sophisticated boundary conditions can be imposed. This makes unnecessary the use of super cells required to simulate finite systems as in plane waves codes. The shape of the simulation region can also be arbitrary selected, reducing the degrees of freedom required for the simulation[7].

- The discretization error can be systematically reduced by decreasing the spacing and increasing the box size[8]. There is no basis superposition error and as the discretization is independent of the atomic positions there is no Pulay forces (the term due to the derivative of the basis set with respect to the atomic positions).

- The number of degrees of freedom is usually similar to plane wave representations and larger than real-space basis sets. But a low amount of work is required for each point and since all operations are local or semi-local a domain decomposition approach can be used for parallelization.

- A particular problem of real-space grids is the breaking of the translation invariance. This is the so called *egg-box effect*, an artificial variation of the energy with respect to relative position between the ions and the grid points. As explained later, this effect can be reduced by a filtering scheme.

B. Pseudopotential approximation

In order to efficiently represent the atomic potential in a real space grid the Troullier-Martins norm conserving pseudo-potentials[46] are used. They are applied in the Kleinman-Bylander[47] form

$$\hat{V}^{ion} = V^{local} + \sum_{lm} \frac{|\psi_{lm}\delta V_l^{nl}\rangle\langle\delta V_l^{nl}\psi_{lm}|}{\langle\psi_{lm}|\delta V_l^{nl}|\psi_{lm}\rangle} \ . \tag{45}$$

As the non-local part is short ranged the integration, is performed in a small spherical grid around the atom. To reduce the *egg-box* effect the Fourier components of the pseudo-

[7] For example simulations in this work were performed using a *minimum box*: a box formed by spheres around each atom. It usually contains half of the points of an equivalent cubic cell.

[8] Unlike the plane wave case, the convergence with the number of degrees of freedom is not variational due to the finite difference approximation.

potentials that cannot be represented in the grid are filtered out using the mask function scheme of Tafipolsky and Schmid[48].

C. Calculation of the Forces

In principle the forces acting over the ions are given by Eq. , however, due to the derivatives of the ionic potential (that can have very high Fourier components), this expression is difficult to calculate accurately on real-space grids. Fortunately an alternative expression in terms of the gradient of the wave-functions can be obtained[45]:

$$\frac{dE}{d\mathbf{R}_J} = 2\sum_A \left[\frac{d\varphi_A^*(\mathbf{r})}{d\mathbf{r}} \hat{V}_J(\mathbf{r}-\mathbf{R}_J)\,\varphi_A(\mathbf{r}) + \varphi_A^*(\mathbf{r})\,\hat{V}_J(\mathbf{r}-\mathbf{R}_J)\,\frac{d\varphi_A(\mathbf{r})}{d\mathbf{r}} \right] . \tag{46}$$

D. Time-propagation

Given an initial condition $\phi(t=0)$ and $R(t=0)$, we want to calculate $\phi(t)$ and $R(t)$ for a time $t>0$ from , this is usually called time propagation or time evolution. The ionic part (Eq. 25) is simple once we get the forces from Eq. (46) and can be treated by the standard velocity Verlet algorithm.

For the electronic part (Eq. 24), due to the transformation (43) we can use the standard Ehrenfest propagation methods, making our scheme trivial to implement in an existing real-time Ehrenfest code.

The key part for the real-time solution of equation (24) is to approximate the propagation operator

$$\varphi(t+\Delta t) = \hat{U}(t+\Delta t, t)\ \varphi(t) \tag{47}$$

in an efficient and stable way. From the several methods available[49], in this work we have chosen the *approximated enforced time-reversal symmetry* (AETRS) method. The propagator is approximated by the explicitly time-reversible expression

$$\hat{U}(t+\Delta t, t) = \exp\left\{-i\frac{\Delta t}{2}\hat{H}(t+\Delta t)\right\}\exp\left\{-i\frac{\Delta t}{2}\hat{H}(t)\right\} , \tag{48}$$

and $\hat{H}(t+\Delta t)$ is obtained from an interpolation from previous steps. For the calculation of the exponential in Eq. (48) a simple fourth order Taylor expansion is used (this particular is order has advantageous numerical properties[49]).

Note that as both the ionic and the electronic methods are time reversible, they do not produce a drift in the total energy that can be present in BOMD implementations [15].

We also implemented the Car-Parrinello scheme to compare it with our approach. In this case the electronic part is integrated by the RATTLE/Velocity Verlet algorithm as described in Ref. [50].

E. Parallelization

In order to tackle large systems and for large times a molecular dynamics method has be run able to run efficiently in parallel architectures. To achieve parallel efficiency we have incorporated a two-way parallelization scheme that may divide the work among a given number of processors, splitting the tasks either in Kohn-Sham states, in regions of real-space, or in a combination of both of them. Each single form of the contemplated parallelizations may scale by its very nature only to a certain maximum number of processors. Only combined schemes allow to overcome such limitations.

Since the propagation step is independent for each orbital, is natural to parallelize the problem by dividing the Kohn-Sham states among processors. Communication is only required once per time-step to calculate quantities that depend on a sum over states: the time dependent densities and the forces over the ions. This type of sum of a quantity over several nodes is known as a reduction and the communication cost grows logarithmically with the number of nodes.

The main limitation to the parallel scalability of this scheme was observed to come from the parts of the code that do not depend on the states (global quantities), mainly the re-generation of the ionic potential

$$V^{ion} = \sum_J V_J^{local} \left(\mathbf{r} - \mathbf{R}_J \right) \tag{49}$$

and the calculation of the forces due to the local part of the ionic potential

$$\mathbf{F}_J^{local} = \int d\mathbf{r} \, \frac{d\rho \left(\mathbf{r} \right)}{d\mathbf{r}} v_J^{local} \left(\mathbf{r} - \mathbf{R}_J \right) \ . \tag{50}$$

As these expressions depend on the atoms index a complementary parallelization in atoms is used to speed up these code sections. For example, to generate the ionic potential, each processor generates the potential for a subset of the atoms and then a reduction operation is performed to obtain the total ionic potential.

As a second parallelization strategy, the real-space mesh can be divided into different domains, so that each processor can treat a different portion of the total mesh. This is illustrated in the left of Fig. 1, where we show a six-fold domain decomposition of a benzene molecule in the x-y plane. Apart from the distribution of the computational burden over the different nodes, this parallelization strategy also has the distinct advantage that the total memory requirement for the storage of the grid points is distributed over the nodes. Much larger systems can be treated if domain parallelization is used.

The price one has to pay for this flexibility is the rather involved implementation which requires non-trivial communication among the nodes. On the right hand side of Fig. 1 we show the application of a finite-difference stencil of the Laplacian to a boundary point of Domain B. Due to the non-local character of the stencil this requires points of Domain A (grey shaded area) which are held in memory and calculated by a neighboring processor. These points are termed ghost points and need to be communicated among neighboring nodes every time the function values on the grid change. To reduce the communication cost an overlap of computation and communication is used. When calculating a derivative over the grid, first the ghost point points are sent, then the derivatives for inner points (i.e. points that do not depend on ghost points) are calculated, after that ghost points are received and finally the calculation of the rest of the points is done. On some computational systems this scheme can completely hide the communication cost for the application of differential operators.

IV. RESULTS

A. Two band model

To illustrate the properties of the new scheme, and also to compare it to CP in a complementary manner to the calculations in the rest of the manuscript, we apply it to a model system. The simple toy model we use is based on the one used in the work by Pastore et al. to test CP [51]. Its EoM are produced by the Lagrangian

$$\begin{aligned} L_{\text{toy}} \;=\; & \frac{\mu}{2}(\dot{\theta}_1\theta_2 - \dot{\theta}_2\theta_1) + \frac{1}{2}M_R\dot{R}^2 + \frac{1}{2}M_G\dot{G}^2 \\ & - \frac{1}{2}K_R(R-R_0)^2 - \frac{1}{2}K_G(G-G_0)^2 + \frac{G}{2}\left[\cos(\theta_1 - R) + \cos(\theta_2 - R)\right] \;, \end{aligned} \tag{51}$$

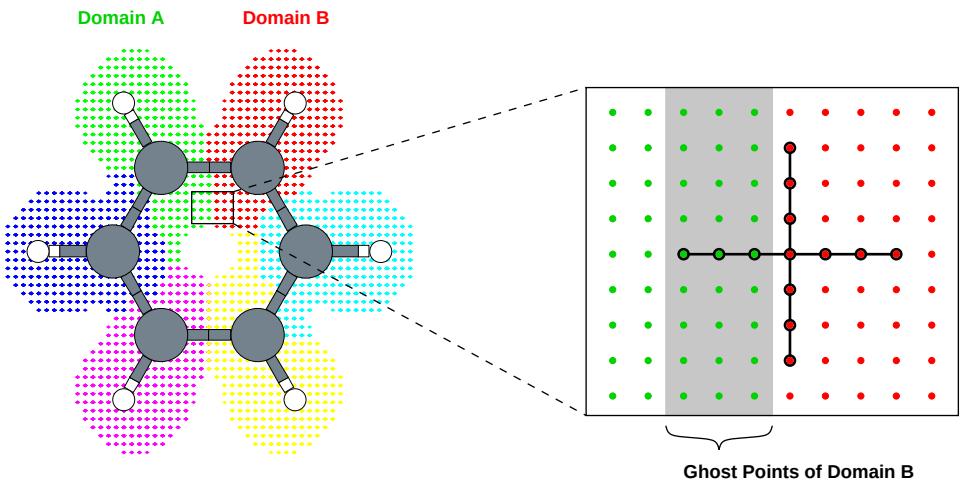

FIG. 1: (left) Example of a real-space grid for a benzene molecule. The grid shape is calculated by placing a sphere around each atom. The different colours show a domain decomposition that can be used to perform the calculation in parallel. (right) Example of ghost points of domain B (see Ref. [42] for details).

where θ_1 and θ_2 correspond to electronic degrees of freedom, R to the nuclear motion and G mimicks the gap. The parameters M_R, K_R, R_0 and G_0 have been taken from the experimental values for the N_2 molecule (interpreting R as the length of the N–N bond).

The dynamics produced by (51) has been then compared to the analogous CP one [obtained by simply changing the θ-kinetic energy by $(\mu_{\rm CP}/2)(\dot\theta_1^2+\dot\theta_2^2)$], and to the gsBO reference [defined by setting $\mu=0$, and θ_1 and θ_2 to the values that minimize the potential energy in (51), $\theta_1=\theta_2=R$]. In all simulations, the initial conditions of R and G have been increased a 10% from their equilibrium values R_0 and G_0, we have set $\dot R(0)=\dot G(0)=0$, and the initial electronic coordinates have been placed at the gsBO minimum (for CP, $\dot\theta_1(0)=\dot\theta_2(0)=0$).

To compare the approximate nuclear trajectory $R(t)$ to the gsBO one $R_{\rm BO}(t)$, we define $d_R=100/\Delta R\left(\frac{1}{T}\int_0^T\left[R(t)-R_{\rm BO}(t)\right]^2{\rm d}t\right)^{1/2}$, where ΔR is the maximum variation of R in the gsBO case. In Fig. 2a, we show that this distance smoothly decreases to zero as $\mu\to 0$ for our model. In Fig. 2b, in turn, we compare the gsBO force on R to the one obtained from the new method averaging over a intermediate time between those associated to the electronic and nuclear motions. The distance d_F between these forces (defined analogously

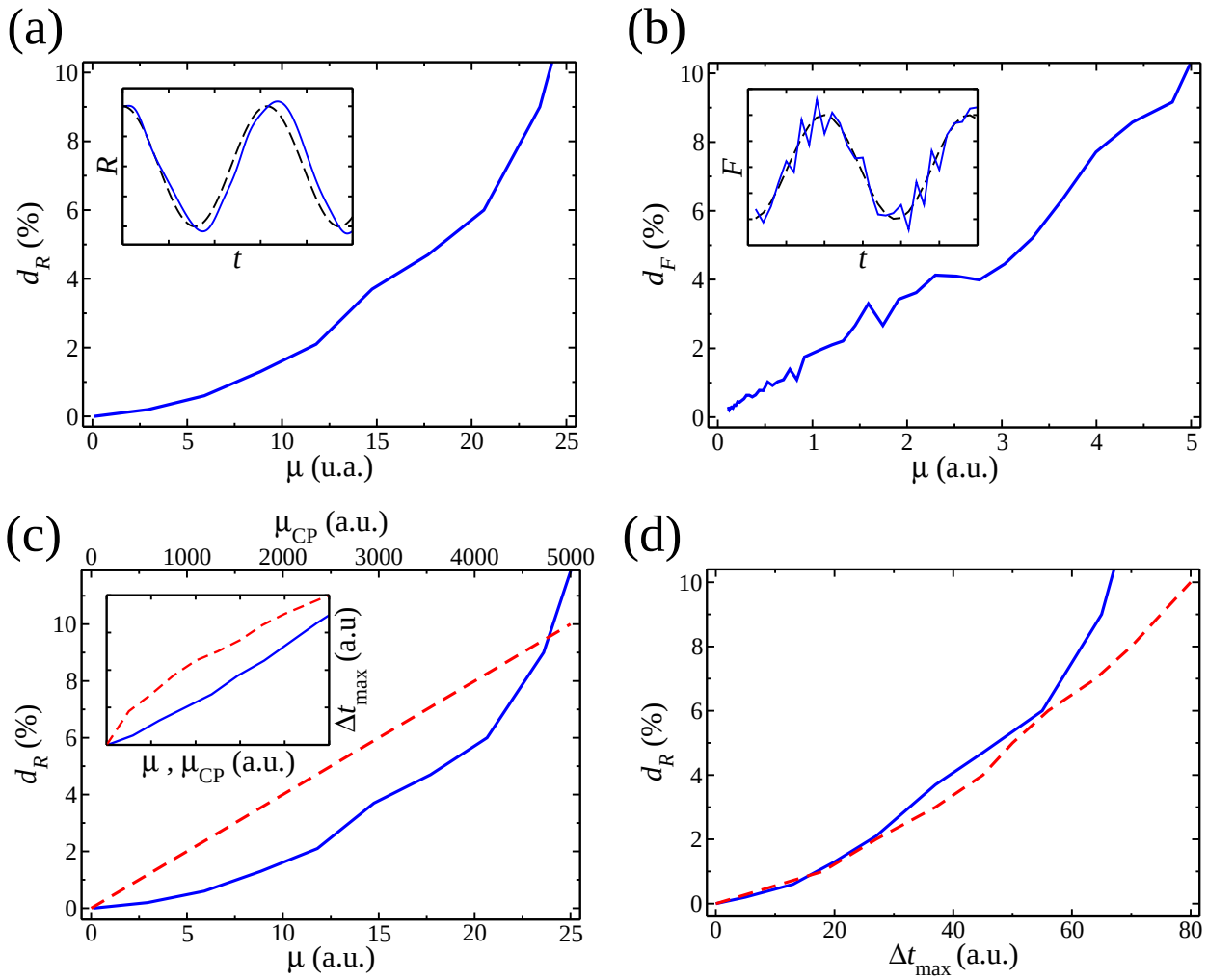

FIG. 2: (a) Distance d_R from the R-dynamics produced by (51) to the gsBO one as a function of μ. Inset: the gsBO R-trajectory [broken (black) line] and the approximate one for $d_R = 10\%$ [solid (blue) line]. (b) Distance between the averaged force on R produced by (51) and the gsBO one. Inset: the gsBO force [broken (black) line] and the approximate one for $d_F = 10\%$ [solid (blue) line]. (c) Dependence on μ (and $\mu_{\rm CP}$) of the distance d_R, and of the maximum ionic time $\Delta t_{\rm max}$ step (inset); for both the new scheme [solid (blue) line] and CP [broken (red) line]. (d) Error/time step profile for both the new dynamics and CP [same keys as in (b)].

to d_R), also goes to zero when $\mu \to 0$.

Now, we estimate the relation between the maximum time step allowed by the fourth order Runge-Kutta numerical integration of the EoM and the error, given by d_R. The first, denoted by $\Delta t_{\rm max}$, has been defined as the largest time step that produced trajectories

for all the dynamical variables of the system with a distance less than 0.1% to the 'exact' trajectories. In Fig. 2c, we can see that, although $\Delta t_{\max}$ grows more slowly in our method than in CP (as expected from the discussion in the previous sections of the paper), the behaviour of the error (d_R) is better for the new dynamics introduced here. These two effects approximately balance each other yielding the error/time step relations depicted in Fig. 2d, where the new scheme is shown to behave similarly to CPMD for a significant range of values of d_R. We stress however that, to actually compare the relative performance of both methods the numerical work required in each time step would have to be considered. In this sense, the more realistic simulations in the next sections are more representative.

B. Nitrogen molecule

For the Nitrogen molecule (N_2), we calculate the trajectories for different values of μ, using the same initial conditions as in the toy model. A time step of $\mu \times 0.0012$ fs is used and the system is propagated by 242 fs. In Fig. 3 we plot the potential energy as a function of the interatomic distance during the trajectory for each run, in the inset we also give the vibrational frequency for the different values of μ, obtained as the position of the peak in the Fourier transform of the velocity auto-correlation function. It is possible to see that for $\mu = 20$ the simulation remains steadily close to the BO potential energy surface and there is only a 3.4% deviation of the vibrational frequency. For $\mu = 30$ the system starts to strongly separate from the gsBO surface by mixing with higher BO surfaces.

C. Benzene

Next, we applied the method to the Benzene molecule. We set-up the atoms in the equilibrium geometry with a random Maxwell-Boltzmann distribution for 300°K. Each run was propagated for a period of time of ~ 400 [fs] with a time step of $\mu \times 0.001$ [fs] (that provide a reasonable convergence in the spectra). Vibrational frequencies were obtained from the Fourier transform of the velocity auto-correlation function. In table I, we show some low, medium and high frequencies of benzene as a function of μ. The general trend is a red-shift of the frequencies with a maximum deviation of 7% for $\mu = 15$. Still, to make a direct comparison with experiment, we computed the infrared spectra as the Fourier

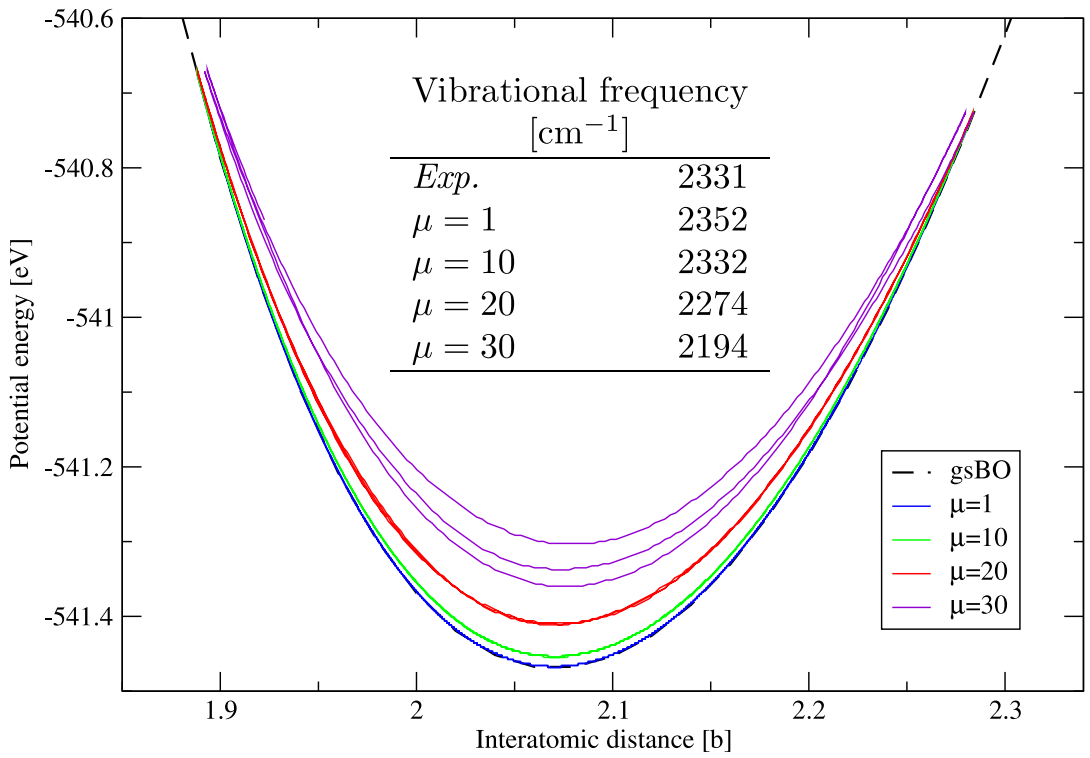

FIG. 3: KS potential energy $E_{\rm KS}[\varphi, R]$ as a function of the internuclear distance R in N_2 molecule simulations. Starting from below, the gsBO result [broken (black) line], and $\mu = 1$ [solid (blue) line], 10 [solid (green) line], 20 [solid (red) line], 30 [solid (violet) line]. Inset: vibrational frequencies from experiment [52] and calculated from the trajectory using different values of μ.

transform of the electronic dipole operator. In Fig. 4, we show how the spectra changes with μ. For large μ, besides the red-shift, spurious peaks appear above the higher vibrational frequency (not shown). We performed equivalent CP calculations for different values of μ_{cp}, and found that, as shown in Fig. 4, it is possible to equiparate the physical error induced in both methods and establish and a relation between μ and μ_{cp}.

Having established the link between μ and μ_{cp} we address the numerical performance of our new method compared to CP in terms of system size. To do this, we simulated several benzene molecules in a cell. For the new scheme, a value of $\mu = 15$ is used while for CP

$\mu = 1$	398	961	1209	1623	3058
$\mu = 5$	396	958	1204	1620	3040
$\mu = 10$	391	928	1185	1611	2969
$\mu = 15$	381	938	1181	1597	2862

TABLE I: Selected vibrational frequencies (in cm^{-1}) for the Benzene molecule, obtained using different values of μ.

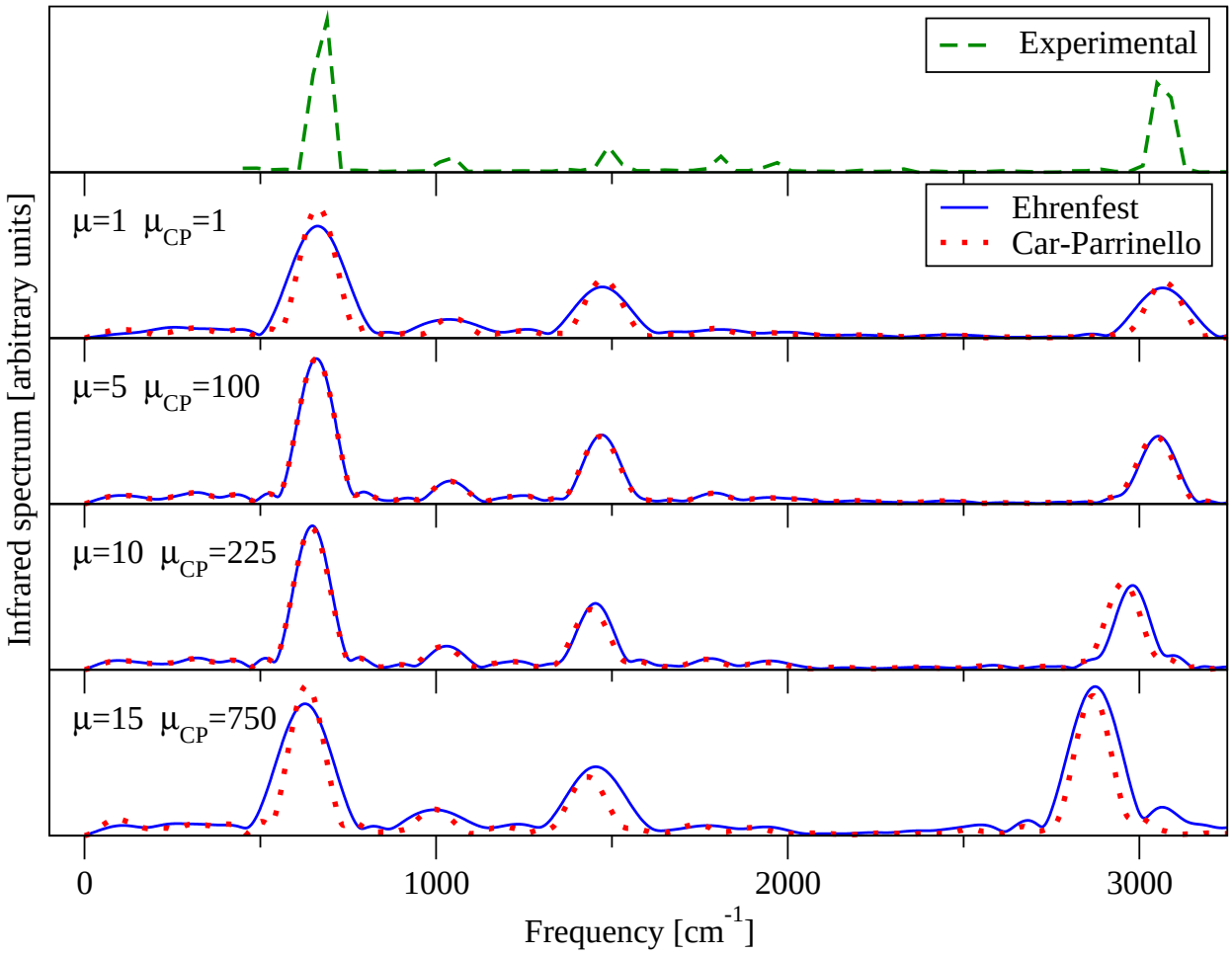

FIG. 4: Calculated infrared spectrum for benzene for different values of μ, compared to CP dynamics and to experiment [53].

$\mu_{cp} = 750$, (values that yield a similar deviation for the BO surface, according to Fig. 4). The time steps used are 3.15 [a.u] and 7.26 [a.u.] respectively. The computational cost is measured as the simulation time required to propagate one atomic unit of time, this is an objective measure to compare different MD schemes. We performed the comparison both

for serial and parallel calculations; the results are shown in Fig. 5. In the serial case, CP is 3.5 times faster for the smaller system, but the difference reduces to only 1.7 times faster for the larger one. Extrapolating the results we predict that the new dynamics will become less demanding than CP for around 1100 atoms. In the parallel case, the performance difference is reduced, being CP only 2 times faster than our method for small systems, and with a crossing point below 750 atoms. This is due to the better scalability of the Ehrenfest approach, as seen on Fig. 5c. Moreover, memory requirements for our approach are lower than for CP: in the case of 480 atoms the ground state calculation requires a maximum of 3.5 Gb whereas in the molecular dynamics, Ehrenfest requires 5.6 Gb while CP 10.5 Gb.

D. Fullerene

To end the computational assessment of the new formalism, we illustrate out method for the calculation of the infrared spectrum of a prototype molecule, C_{60}. We use a value of $\mu = 5$. The calculated IR spectra is in very good agreement with the experiment (see Fig. 6) for low and high energy peaks (the ones more sensitive to the values of μ as seen in Fig. 4). The result is robust and independent of the initial condition of the simulation. The low energy splitting of IR spectrum starts to be resolved for simulations longer than 2 [ps].

V. CONCLUSIONS

In conclusion, we have presented a new approach to AIMD based on a generalization of TDDFT Ehrenfest dynamics. Our approach introduces a parameter μ that for particular values recovers not only Ehrenfest dynamics but also Born-Oppenheimer dynamics. In general μ controls the trade-off between the closeness of the simulation to the BO surface and the numerical cost of the calculation (analogously to the role of the fictitious electronic mass in CP). We have shown that for a certain range of values of μ the dynamic of the fictitious system is close enough to the Born-Oppenheimer surface while allowing for a good numerical performace.

We have made direct comparisons of the numerical performance with CP, and, while quantitatively our results are system- and implementation-dependent, they prove that our method can outperform CP for some relevant systems. Namely, large scale systems that are

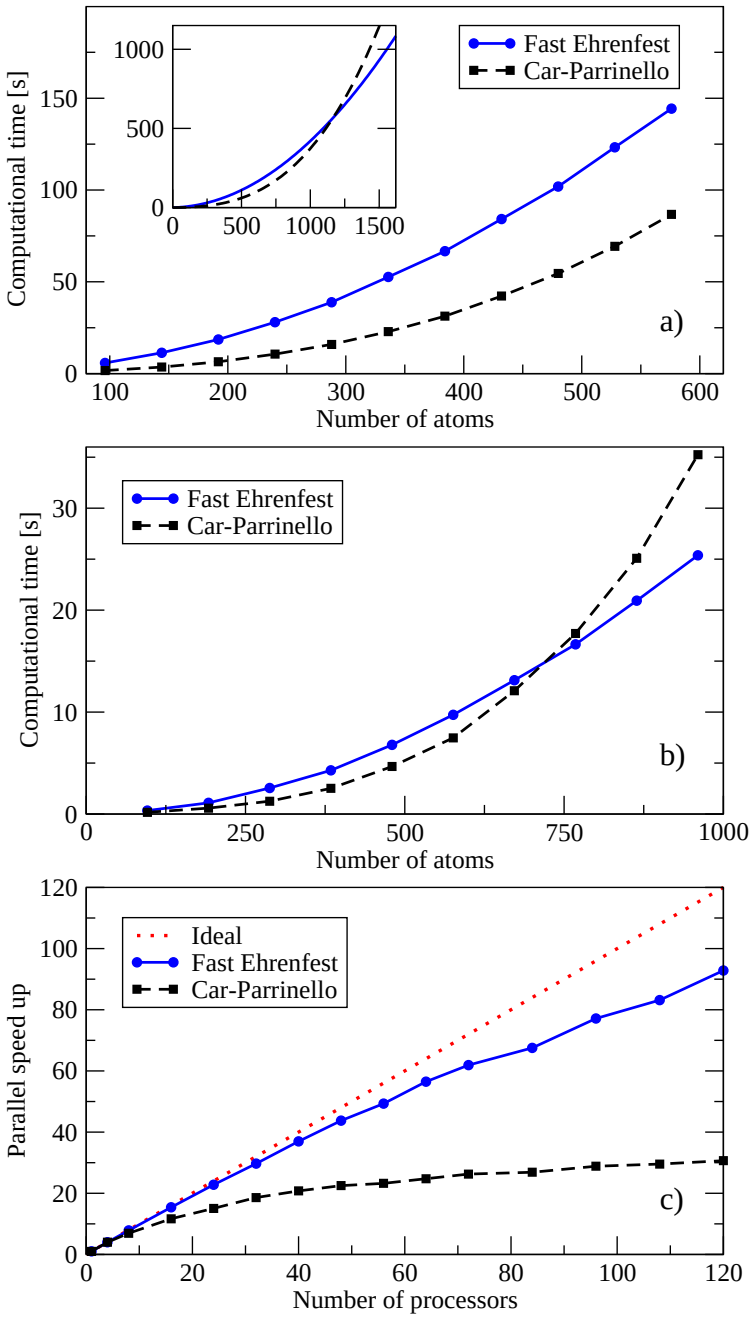

FIG. 5: Computational performance comparisons of our method and CP for an array of benzene molecules with finite boundary conditions and a spacing of 0.6 [a.u.]. Performance is measured as the computational time required to propagate one atomic unit of time. a) Single processor computational cost for different system sizes. (inset) Polynomial extrapolation for larger systems. Performed in one core of an Intel Xeon E5435 processor. b) Parallel computational cost for different system sizes. Performed in $32 \times$ Intel Itanium 2 (1.66 GHz) processor cores of a SGI Altix. c) Parallel scaling with respect to the number of processor for a system of 480 atoms in a SGI Altix system. In both cases a mixed states-domain parallelization is used to maximize the performance.

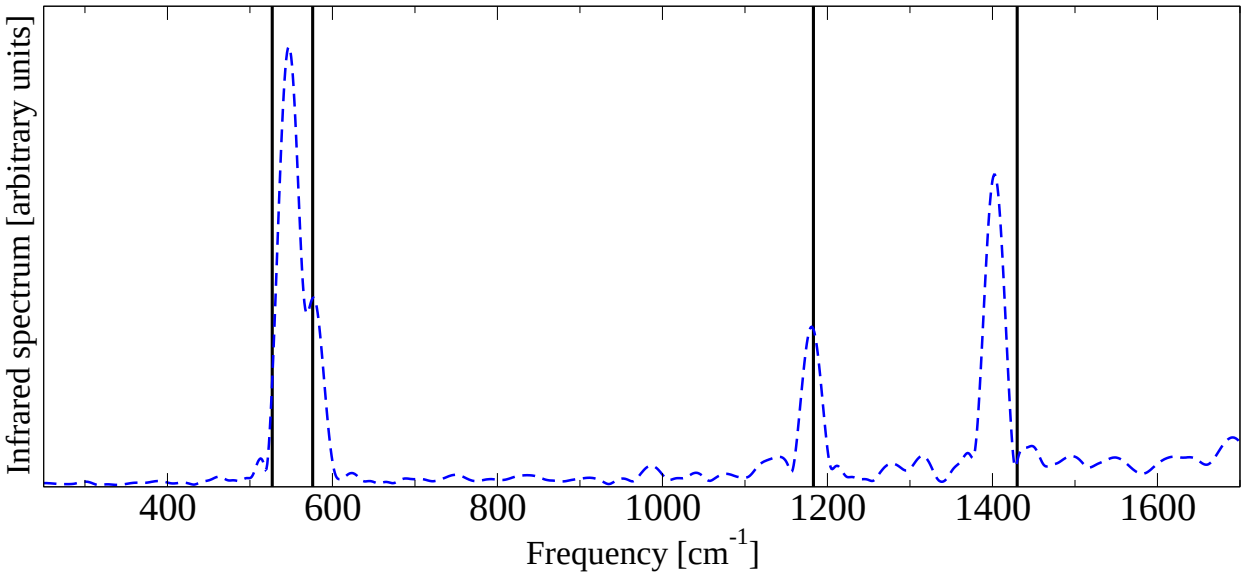

FIG. 6: Infrared spectrum of C_{60}. The (blue) dashed line corresponds to the calculated one (μ=5 and 2 [ps] of time) while the black bars are the experimental values from Ref. [54].

of interest in several research areas and that can only be studied from first principles MD in massively parallel computers. To increase its applicability it would be important to study if the improvements developed to optimize CP can be combined with our approach [55], in particular techniques to treat small gap or metallic systems [56].

Finally, note that the introduction of the parameter μ comes at a cost, as we change the time scale of the movements of the electrons with respect to the Ehrenfest case, which implies a shift in the electronic excitation energies. This must be taken into account to extend the applicability of our method for non-adiabatic MD and MD under electromagnetic fields, in particular for the case of Raman spectroscopy, general resonant vibrational spectroscopy as well as laser induced molecular bond rearrangement.

Another important aspect of the specific examples discussed in this article is related to the fact that electron dynamics are usually determined quantum mechanically but the nuclear motion is treated within the framework of classical mechanics. Despite a large difference in the general time scales of electronic and nuclear motions, electronic wavepackets quite often couple with the dynamics of nuclear motion. The proper incorporation of the electronic response is crucial for describing a host of dynamical processes, including laser-induced chemistry, dynamics at metal or semiconductor surfaces, and electron transfer in molecular, biological, interfacial, or electrochemical systems (in particular it is crucial also

for describing light-induced processes in biomolecules, and many other photochemical reactions). The two most widely used approaches to account for non-adiabatic effects are the surface-hopping method and the Ehrenfest method implemented here. The surface-hopping approach extends the Born-Oppenheimer framework to the non-adiabatic regime by allowing stochastic electronic transitions subject to a time- and momenta-dependent hopping probability. On the other hand Ehrenfest successfully adds some non-adiabatic features to molecular dynamics but it is rather incomplete. This approximation can fail either when the nuclei have to be treated as quantum particles (e.g. tunnelling) or when the nuclei respond to the microscopic fluctuations in the electron charge density (heating) not reproducing the correct thermal equilibrium between electrons and nuclei (which constitutes a fundamental failure when simulating the vibrational relaxation of biomolecules in solution). However there have been some proposals in the literature to include some of those effects in a modified Ehrenfest scheme [57, 58] or beyond it (see, e.g. Ref. [59]).

On a more practical level an extremely important and yet open question is how to obtain the excite state of a given system in TDDFT?. This question is of paramount relevance if one wishes to do excited state dynamics in a given excited state. At present there is no satisfactory solution to this problem and most calculations are indeed approximative, by either assuming that a given population of single Kohn-Sham orbitals can mimic and exited state or by constructing some approximation to it. Ideally TDDFT can provide you that state by either tailoring an external laser that maximize the population of a desired excited state In this context all non-linear phenomena related to higher-oder response functions of high intense laser pulses might require the development of exchange-correlation functionals that are non only spatially non-local but also have strong memory effects. What are the impact of those effects in the excited state properties of biomolecules is still in its infancy.

Acknowledgements

The author would like to acknowledge his thesis supervisors Angel Rubio (UPV/EHU) and Silvana Botti (Ecole Polytechnique, Paris). He would also like to acknowledge his collaborators: Alberto Castro (Freie Universität, Berlin), Pablo Echenique, Diego Prada, Fernado Falceto and José Luis Alonso (Universidad de Zaragoza) and David Zueco (Universität Augsburg). Finally I would also like to thank the help of Carolina Román, Miguel

Marques, Florian Lorenzen and Nicole Helbig.

This work was made possible by the following proyects: MEC: FIS2006-12781-C02-01, FPA2006-02315, FIS2007-65702-C02-01, BFM2002-00113; EC: Nanoquanta (NMP4-CT-2004-500198), and e-I3 (INFRA-211956); UPV/EHU (SGIker Arina) and Barcelona Supercomputing Center.

---

[1] N. Metropolis, A. W. Rosenbluth, M. N. Rosenbluth, A. H. Teller, and E. Teller, J. Chem. Phys. **21**, 1087 (1953).

[2] J. D. Bernal, Nature **183**, 141 (1959).

[3] B. J. Alder and T. E. Wainwright, J. Chem. Phys. **31**, 459 (1959).

[4] E. Fermi, J. Pasta, S. Ulam, and M. Tsingou, *Studies of nonlinear problems I*, Los Alamos Scientific Laboratory Report #LA-1940 (1955).

[5] J. Ford, Phys. Rep. **213**, 271 (1992).

[6] G. Ciccotti, D. Frenkel, and I. McDonald, *Simulations of liquids and solids: molecular dynamics and motecarlo methods in statistical mechanics* (North-Holand, Amsterdam, 1987).

[7] A. Warshel and W. R. M., J. Chem. Phys. **102**, 6218 (1980).

[8] D. Marx and J. Hutter, in *Modern Methods and Algorithms of Quantum Chemistry*, edited by J. Grotendorst (John von Neumann Institute for Computing, Jülich, 2000), vol. 3, pp. 329–477.

[9] M. E. Tuckerman, J. Phys.: Condens. Matter **14**, R1297 (2002).

[10] C. Fiolhais, F. Nogueira, and M. Marques, eds., *A Primer in Density Functional Theory*, Lecture Notes in Physics (Springer-Verlag, Berlin, Heidelberg, 2003).

[11] P. Hohenberg and W. Kohn, Phys. Rev. **136**, B864 (1964).

[12] W. Kohn, Rev. Mod. Phys. **71**, 1253 (1999).

[13] W. Kohn and L. J. Sham, Phys. Rev. **140**, A1133 (1965).

[14] R. Car and M. Parrinello, Phys. Rev. Lett. **55**, 2471 (1985).

[15] A. M. N. Niklasson, C. J. Tymczak, and M. Challacombe, Phys. Rev. Lett. **97**, 123001 (2006).

[16] W. Andreoni, D. Marx, and M. Sprik, ChemPhysChem **6**, 1671 (2005), and references therein.

[17] S. Goedecker, Rev. Mod. Phys. **71**, 1085 (1999).

[18] T. D. Kühne, M. Krack, F. R. Mohamed, and M. Parrinello, Phys. Rev. Lett. **98**, 066401

(2007).

[19] L. Brillouin, Chem. Rev. **183**, 24 (1926).

[20] H. A. Kramers, Z. Phys. **39**, 828 (1926).

[21] G. Wentzel, Z. Phys. **38**, 518 (1926).

[22] M. A. L. Marques, C. A. Ullrich, F. Nogueira, A. Rubio, K. Burke, and E. K. U. Gross, eds., *Lecture Notes in Physics*, vol. 706 (Springer-Verlag, Berlin, Heidelberg, 2006).

[23] E. Runge and E. K. U. Gross, Phys. Rev. Lett. **706**, 997 (1984).

[24] J. L. Alonso, X. Andrade, P. Echenique, F. Falceto, D. Prada-Gracia, and A. Rubio, Phys. Rev. Lett. **101**, 096403 (2008).

[25] P. Echenique and J. L. Alonso, Mol. Phys. **105**, 3057 (2007).

[26] R. B. Gerber, V. Buch, and M. A. Ratner, J. Chem. Phys. **77**, 3022 (1982).

[27] R. B. Gerber and M. A. Ratner, Adv. Chem. Phys. **70**, 97 (1988).

[28] F. A. Bornemann, P. Nettesheim, and C. Schütte, *Quantum-classical molecular dynamics as an approximation to full quantum dynamics*, Preprint SC 95-26, Konrad-Zuse-Zentrum für Informationstechnik Berlin (1995).

[29] F. A. Bornemann, P. Nettesheim, and C. Schütte, J. Chem. Phys. **105**, 1074 (1996).

[30] P. G. P, Z. Phys. **73**, 169 (1931).

[31] D. B. Wallace, Master's thesis, University of Central Florida, Orlando, Florida (2005).

[32] H. Hellmann, *Einführung in die quantenchemie*, Leipzig, Frank Deuticke, p. 285 (1937).

[33] R. P. Feynman, Phys. Rev. **56**, 340 (1939).

[34] J. L. Tully, in *Classical and Quantum Dynamics in Condensed Phase Simulation*, edited by B. J. Berne, G. Ciccotti, and D. F. Coker (World Scientific, Singapore, 1998), pp. 489–515.

[35] P. Grochowski and B. Lesyng, J. Chem. Phys. **119**, 11541 (2003).

[36] T.-C. Li and P. Tong, Phys. Rev. A **34**, 529 (1986).

[37] E. Runge and E. K. U. Gross, Phys. Rev. Lett. **52**, 997 (1984).

[38] E. K. U. Gross, J. F. Dobson, and M. Petersilka, in *Density Functional Theory*, edited by Nalewajski (Springer-Verlag, Berlin, Heidelberg, 1996), vol. 181 of *Topics in Current Chemistry*, pp. 81–172.

[39] J. P. Perdew and A. Zunger, Phys. Rev. B **23**, 5048 (1981).

[40] J. Theilhaber, Phys. Rev. B **46**, 12990 (1992).

[41] R. K. Kalia, P. Vashishta, L. H. Yang, F. W. Dech, and J. Rowlan, Intl. J. Supercomp. Appl.

4, 22 (1990).

[42] A. Castro, M. A. L. Marques, H. Appel, M. Oliveira, C. A. Rozzi, X. Andrade, F. Lorenzen, G. E. K. U., and A. Rubio, Phys. Status Solidi B **243**, 2465 (2006).

[43] M. A. L. Marques, A. Castro, G. F. Bertsch, and A. Rubio, Comput. Phys. Commun. **151**, 60 (2003).

[44] J. R. Chelikowsky, N. Troullier, and Y. Saad, Phys. Rev. Lett. **72**, 1240 (1994).

[45] K. Hirose, T. Ono, Y. Fujimoto, and S. Tsukamoto, *First-Principles Calculations in Real-Space formalism* (Imperial College Press, London, 2005).

[46] N. Troullier and J. L. Martins, Phys. Rev. B **43**, 1993 (1991).

[47] L. Kleinman and D. M. Bylander, Phys. Rev. Lett. **48**, 1425 (1982).

[48] M. Tafipolsky and R. Schmid, J. Chem. Phys. **124**, 174102 (2006).

[49] A. Castro, M. A. L. Marques, and A. Rubio, J. Chem. Phys. **121**, 3425 (2004).

[50] M. E. Tuckerman and M. Parrinello, J. Chem. Phys. **101**, 1316 (1994).

[51] G. Pastore, E. Smargiassi, and F. Buda, Phys. Rev. A **44**, 6334 (1991).

[52] M. F. Crawford, H. L. Welsh, and J. L. Locke, Phys. Rev. **75**, 1607 (1949).

[53] S. S. director NIST Mass Spec Data Center, *NIST Chemistry WebBook, NIST Standard Reference Database Number 69* (National Institute of Standards and Technology, Gaithersburg MD, 20899, USA, 2005), chap. Mass Spectra.

[54] T. Cabioc'h, A. Kharbach, A. Le Roy, and J. P. Rivire, Chem. Phys. Lett. **285**, 216 (1998).

[55] T. D. Kuhne, M. Krack, F. R. Mohamed, and M. Parrinello, Phys. Rev. Lett. **98**, 066401 (2007).

[56] N. Marzari, D. Vanderbilt, and M. C. Payne, Phys. Rev. Lett. **79**, 1337 (1997).

[57] A. Bastida, C. Cruz, J. Z. niga, A. Requena, and B. Miguel, J. Chem. Phys. **126**, 014503 (2007).

[58] K. Takatsuka, J. Phys. Chem. A **111**, 10196 (2007).

[59] A. P. Horsfield, D. R. Bowler, H. Ness, C. G. Sánchez, T. N. Todorov, and A. J. Fisher, Rep. Prog. Phys. **69**, 1195 (2006).